Journal of Power Sources 196 (2011) 6915–6919

Contents lists available at ScienceDirect

Journal of Power Sources

journal homepage: www.elsevier.com/locate/jpowsour

Short communication

A three-dimensional tin-coated nanoporous copper for lithium-ion battery anodes

Shichao Zhang[a,*], Yalan Xing[a], Tao Jiang[a], Zhijia Du[a], Feng Li[a], Lei He[a], Wenbo Liu[b]

[a] School of Materials Science and Engineering, Beijing University of Aeronautics and Astronautics, Beijing 100191, China
[b] School of Manufacturing Science and Engineering, Sichuan University, Chengdu 610065, China

ARTICLE INFO

Article history:
Received 19 September 2010
Received in revised form
22 November 2010
Accepted 8 December 2010
Available online 21 December 2010

Keywords:
Nanoporous
3D structure
Bimodal pore size distributions
Lithium-ion battery

ABSTRACT

Nanoporous copper (NPC), as a new kind of porous metal prepared by dealloying, is introduced into the lithium-ion battery as both the current collector and substrate of active material. The nanoporous copper has three-dimensional structure composed of large channels (hundreds of nanometers) and small pores (tens of nanometers) on the channel walls. Anodes were prepared by electroless depositing of a thin layer of tin on NPC and copper foil. By comparing the electrochemical performance of both electrodes, the nanostructured electrode exhibits much higher areal capacity and better Coulombic efficiency than planar electrode.

1. Introduction

As the increase of demand for advanced electrical vehicles and mobile electronic device power back-ups, lithium-ion batteries are challenged to explore electrodes with higher energy density. Metal based anodes, like Sn, Sb and Si, have attracted much attention because of their higher specific capacities than graphite electrodes [1,2]. However, such materials are known to suffer from dramatic volume expansion during lithiation process which leads to pulverization and poor cycle life [3–5]. Possible solutions include using active/inactive composite as strain buffer [6–8], adopting three-dimensional current collector [9,10] and reducing the size of active material to nano-scale [11–13]. Nanostructured material have unique advantages in mass transport which leads to easy diffusion of electron and lithium-ion, higher electrode/electrolyte interfacial contact area and better accommodation of structural strain during lithiation/delithiation reactions [14]. Simon and his co-workers reported a nano-architectured electrode obtained by depositing pure tin on copper nanopillars [15] and it exhibits good cycle performance.

Recently, nanoporous metal (NPM) prepared by dealloying is a research field drawing increasing attention for its potentials to be employed in many technological applications, such as catalysis, sensors, actuators, fuel cells and so forth [16–19]. Dealloying is a corrosion process during which the less noble element is selectively dissolved from the alloy and forms a homogeneous porous structure [20]. Starting from Ag–Au alloy, various alloy systems have been utilized to study the nanoporosity evolution upon dealloying [20–22]. Nanoporous gold (NPG) with bimodal channel size distributions was synthesized by dealloying Al–Au alloy, which was composed of large-sized channels with highly porous channel walls [23]. Though nanoporous metals have previously shown many achievements, they have not been introduced into lithium-ion batteries.

In this article, we propose a strategy to prepare a three-dimensional (3D) porous anode for lithium-ion batteries by coating a thin layer of tin on nanoporous copper (NPC). The NPC is fabricated by a simple one-step dealloying of Al–Cu alloy and composed of large-sized channels and small pores on the channel walls. The obtained tin-coated NPC (Sn @ NPC), as an active/inactive composite, could take advantage of the nanoporous structure for better mass transport and accommodation of the mechanical strains occurring during cycling. This nano-architectured electrode is meaningful in the design of new lithium-ion battery technologies, especially for 3D nanobatteries.

2. Experimental

The precursor Al–Cu alloy was prepared by melting pure copper (99.99 wt%) and pure aluminum (99.9 wt%) in quartz crucibles by voltaic arc heating in the designed proportion, namely Al

* Corresponding author. Tel.: +86 10 82338148; fax: +86 10 82339319.
E-mail addresses: csc@buaa.edu.cn (S. Zhang), xingyalan@mse.buaa.edu.cn (Y. Xing).

0378-7753/$ – see front matter © 2010 Elsevier B.V. All rights reserved.
doi:10.1016/j.jpowsour.2010.12.021

Table 1
Composition of the electroless plating bath.

Components	Concentration
$SnSO_4$	0.3 M
NaOH	2.8 M
NaH_2PO_4	0.9 M
Sodium citrate	0.6 M

25 at% Cu with the protection of argon atmosphere. Since the alloy ingots were slowly cooled down in the crucibles, the process could be considered as equilibrium solidification. The Al–Cu ingots were then processed into slices by wire-cutting EDM with the thickness of about 200 μm. Prior to further treatment, the slices were washed and polished to remove oil and molybdenum oxides formed on the surface during processing. The dealloying of Al–Cu alloy was performed in 1 M aqueous NaOH solution at room temperature until no obvious air bubbles came out. The samples were then rinsed with distilled water and dehydrated alcohol. After dried in a vacuum oven, a slice of nanoporous copper was obtained.

To prepare tin-coated NPC (Sn @ NPC), electroless plating of tin was conducted in a bath composed of $SnSO_4$, NaOH, NaH_2PO_2 and sodium citrate as listed in Table 1. Typical depositions were carried out at 80 °C for 15 min. When preparing anode for Li-ion battery, a copper adhesive tape was used as a base to support Sn @ NPC slice in case that the slice would crack during the cell-assembling. In order to understand the effect of NPC substrate on cell performance, a tin-coated planar copper foil (Sn @ CF) was fabricated in the same plating bath for 5 min to prepare a tin-coating with similar thickness. The testing half-cells of both kinds of electrodes were assembled in an Ar filled glove box (MB-10-G with TP170b/mono, MBRAUN) with a lithium sheet as a counter and reference electrode. Electrolyte was 1 M $LiPF_6$ in a mixed solution of EC and DEC (1:1 in volume ratio). Each cell was aged for 20 h at room temperature before commencing the electrochemical tests. The galvanostatic measurements were carried out in a battery test system (NEWARE BTS-610, Newware Technology Co., Ltd., China). We choose to report the capacitance of these electrodes in mAh cm^{-2}, area being footprint area of the electrode. The electrochemical performance of Sn @ NPC is presented in comparison with planar Sn @ CF electrode.

Structural characterization and analysis of the Al–Cu alloys, as-dealloyed NPC and tin-coated samples were made using X-ray diffraction (XRD, Rigaku D/Max-2400) with Cu Kα radiation, scanning electron microscopy (SEM, Hitachi S-4800) with an energy dispersive X-ray analyzer (EDS), and transmission electron microscopy (TEM, JEOL JEM 2100F). The cross-section of Sn @ CF was polished by JEOL IB-09010CP for SEM observation.

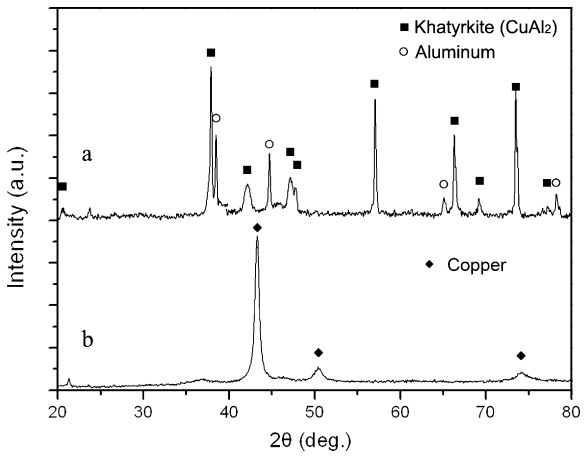

Fig. 1. XRD patterns of (a) Al–Cu precursor alloy, (b) as-dealloyed NPC.

3. Results and discussion

Fig. 1 shows the XRD results of the precursor Al–Cu alloy and dealloyed NPC sample. As displayed in Fig. 1a, the Al–Cu alloy is composed of Al and $CuAl_2$ phases. According to Al–Cu phase diagram [24], $Al_{75}Cu_{25}$ alloy lies between the eutectic composition and intermetallic $CuAl_2$ composition. Based on the theories of equilibrium solidification, some Al_2Cu islands would emerge first, and then Al and Al_2Cu begin to simultaneously precipitate. This could be confirmed by the following SEM analysis. Fig. 1b is the XRD pattern of as-dealloyed NPC sample. Only copper is detected in NPC, implying Al was completely dissolved during dealloying.

The nanoporous microstructure of as-dealloyed NPC is exhibited in Fig. 2. Two regions with different morphologies are observable in Fig. 2a. One is featured with periodic structure of alternating channels and walls in the scale of hundreds of nanometers. Among them is some island-like structure in elliptical shape. This special morphology is originated from the phase structure of precursor alloy. According to the solidification process of Al–Cu alloy, the $CuAl_2$ crystallize to islands first from the melt, and then Al and $CuAl_2$ began to precipitate together at the eutectic point which forms lamella structure. The resulting lamella structure is composed of alternating pure Al and $CuAl_2$ layers. During dealloying, the lamellae of Al were selectively dissolved since Al is a more active element than Cu and channels were left in the resulting structure. Furthermore, the aluminum element in the $CuAl_2$ was also dissolved, leaving voids in the channel walls and islands. In the magnified image, Fig. 2b displays that the channel walls consist of open, three-dimensional (3D) nanoporous structure with pores and ligaments of 10–50 nm width. The insert in Fig. 2b is a magni-

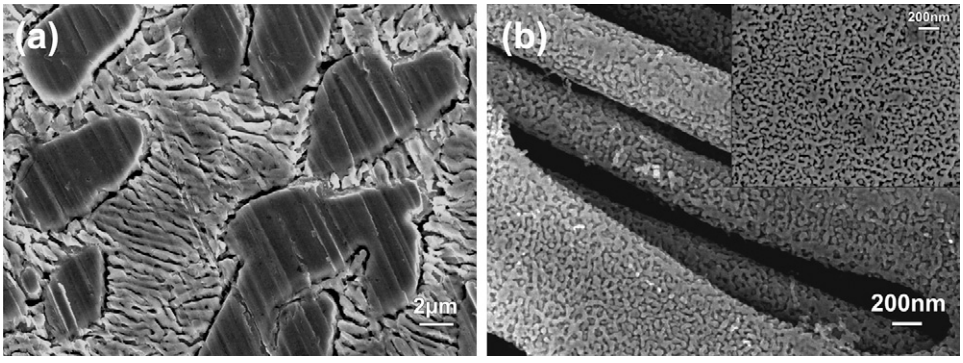

Fig. 2. SEM micrographs of the NPC dealloyed from Al–Cu alloy. (a) Low-magnified image of the overall morphology, consisting of lamella and island-like structure, (b) magnified image of the lamella structure, the insert in (b) is a magnified image of island-like structure.

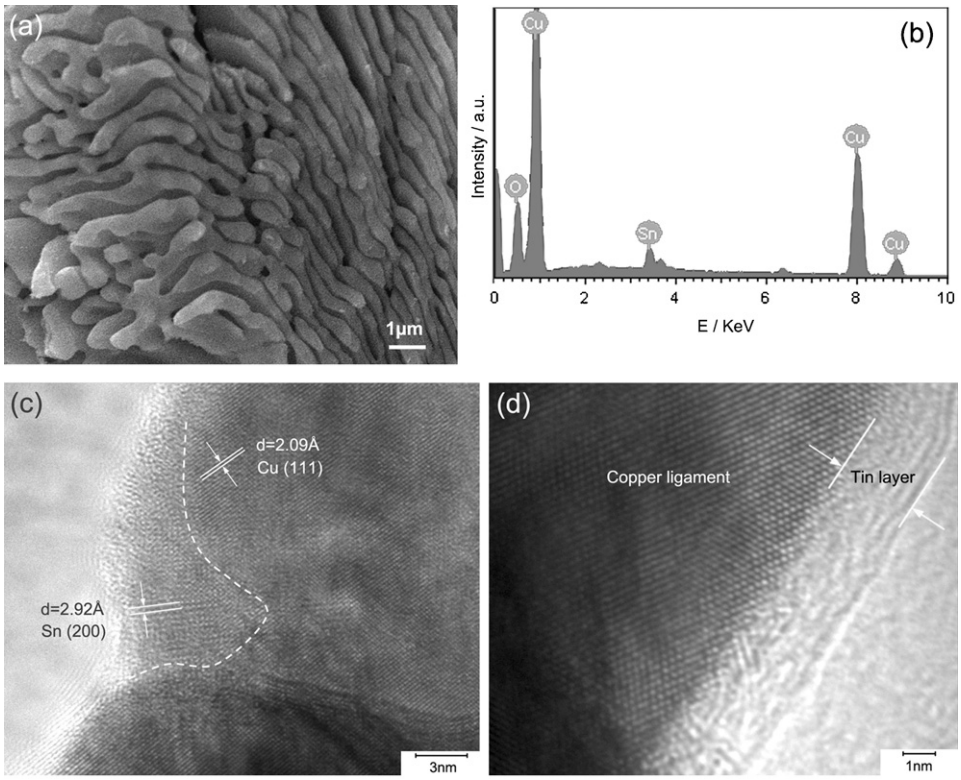

Fig. 3. (a) SEM images of the surface morphology of as-prepared Sn @ NPC. (b) EDS analysis results of the surface of Sn @ NPC. (c) TEM image of Sn @ NPC. By calculating the lattice fringe spacing, tin and copper lattice are distinguished and their interface is marked by white dashed line. (d) A typical TEM image of a tin-covered Cu ligament in Sn @ NPC.

fied image of the island-like region that shows a similar nanoporous structure with the channel walls. This uniformly nanoporous structure is consistent with the reported nanoporous gold [20,25]. It has been reported to prepare nanoporous metals with multimodal pore size distribution [26], but its method including annealing and redealloying is rather complicated. Here, through a simple one-step dealloying method, a nanoporous structure with bimodal pore size distributions is obtained: the large-sized channels are hundreds of nanometers in width, while the small-sized pores on both channel walls and islands are tens of nanometers.

The Sn @ NPC as shown in Fig. 3a was obtained by electroless plating of Sn on the NPC. No obvious morphology changes are observed on the surface comparing with NPC. However, EDS analysis (Fig. 3b) indicates tin has been coated on NPC. TEM observation reveals that a thin layer of tin deposited on NPC as displayed in Fig. 3c. Two sets of lattice fringes with different fringe spacing can be distinguished by the white dashed line. The fringe space of lattice in the right part is 2.09 Å, in agreement with fcc Cu (1 1 1), while the fringe space in the left part is 2.92 Å, in accordance with tetragonal β-Sn (200). Fig. 3d is a typical micrograph of a ligament in the nanoporous structure of Sn @ NPC. It could be clearly identified that a layer of tin exists on the surface of the copper ligament with the thickness of only 3 nm. This indicates that the Tin has been thoroughly and evenly deposited into the inner side of NPC. Compared with the reported Au @ NPC [19] in which the gold thin films grow epitaxially on the copper ligament substrate, the tin film did not show a coherent orientation from the NPC ligament. This is probably because the significant differences of tin and copper in crystal system and cell parameters.

Planar copper foils were also plated with tin (Sn @ CF) in the same method in order to contrast with Sn @ NPC. Fig. 4d exhibits an SEM image of the cross section of obtained Sn @ CF that was plated for 5 min. The bright layer on the top is a tin layer with a thickness about 30 nm which is thicker than that on NPC. However, this is a comparatively thin film as produced by electroless plating on planar foil. Besides, the tin layer is compact and has good contact with copper substrate since no lamination is observed around the interface. Therefore, this Sn @ CF could be used as a reference to evaluate the performance of Sn @ NPC.

Fig. 4a and c show charge–discharge curves of the 1st, 2nd, 10th cycle of Sn @ NPC and Sn @ CF electrodes that tested at a current density of 150 mA g^{-1} between 1.5 V and 0.01 V. According to the first discharge of Sn @ NPC electrode as well as its differential curve displayed in Fig. 4b, two plateaus around 0.2 and 0.5 V can be clearly identified, which are ascribed to lithium insertion into different Li_xSn phases [3,27]. An irreversible plateau above 1.0 V, corresponding to the vague 1.2 V peak in Fig. 4b, is assigned to the formation of a solid electrolyte interphase (SEI) layer due to decomposition of electrolyte on the Sn surface [28,29]. During charge, Sn @ NPC shows a slope ranging from 0.5 to 0.8 V, corresponding to reversible delithiation from Li–Sn alloy. In addition, a slope appears at around 1.3 V which is most likely to be caused by the partially reversible reaction of SnO_x to get reoxidized. Generally, SnO_2 is reduced to tin and forms lithium oxide at 0.7–0.9 V in the first discharge and this process could be partially reversible in the charge which exhibits a broad but weak peak at around 1.3 V [30,31]. In the case of Sn @ NPC, a small amount of tin oxide is possibly formed on the surface. During the discharge, the plateau of tin oxide's reduction cannot be identified since it merged with the plateau of electrolyte decomposition and SEI formation. Nevertheless, a slope at around 1.3 V emerged in the charge process.

The first discharge curve of Sn @ CF electrode also exhibits reversible plateaus at 0.2 and 0.5 V. However, a hump causing irreversible capacity appeared at around 1.5 V. It has been reported that such high-voltage irreversible capacity is associated with the catalytic decomposition of the electrolyte by the tin surface [29,32].

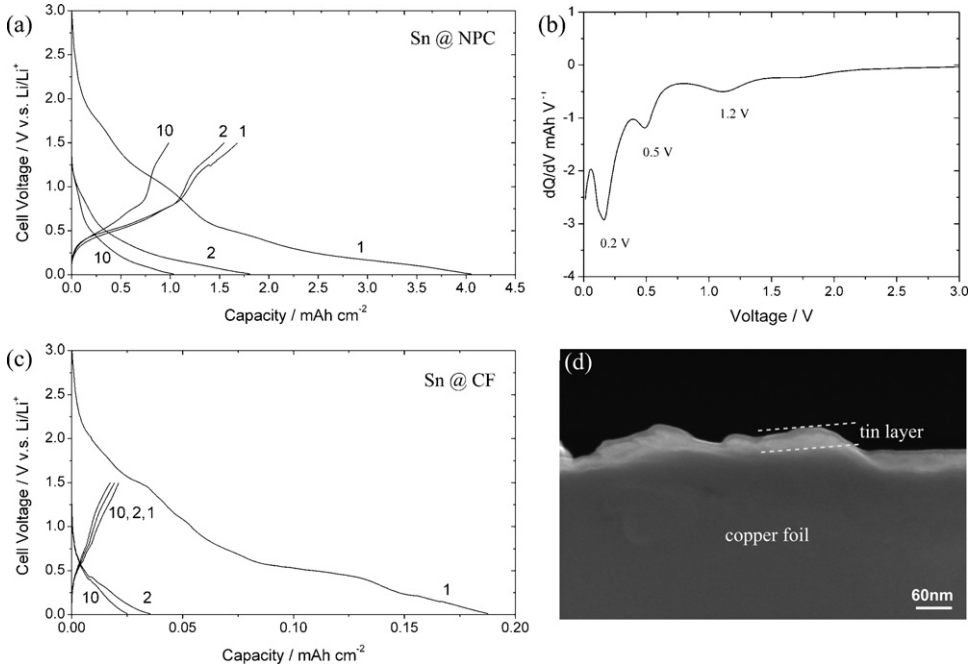

Fig. 4. (a and c) Charge–discharge curves of Sn @ NPC and Sn @ CF electrodes in the 1st, 2nd and 10th cycles at a current density of 150 mA g^{-1} between 0.01 and 1.5 V. (b) Differential curve of the 1st discharge of Sn @ NPC. (d) SEM image of the cross section of Sn @ CF.

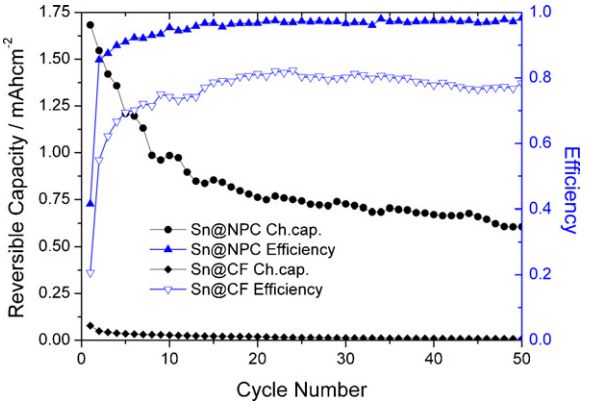

Fig. 5. Cycle performances of Sn @ NPC and Sn @ CF electrodes.

The decomposed electrolyte will form a layer on the tin that hinders the transport of Li ions and causes capacity fading. As a result, the following charge and discharge capacity is less than 18.6% of the first discharge capacity.

The first discharge capacity of Sn @ NPC is 4.05 mA h cm^{-2}, while the second is 1.81 mA h cm^{-2} and the tenth is 1.03 mA h cm^{-2} which are 44.7% and 25.4% of the initial capacity, respectively. The Sn @ CF has only a capacity of 0.188 mA h cm^{-2} in the first discharge, about 1/20 of that of Sn @ NPC. The capacity of Sn @ CF in the following cycles is even less. Therefore, Sn @ NPC electrode has much higher capacity and better capacity retention over Sn @ CF.

Generally, the voltage profiles of Sn @ NPC and Sn @ CF are comparatively smooth without sharp plateaus. This may be caused by the nano-scaled tin film that lead to the decrease of crystal size and partial crystallization. Similar phenomena were observed in other works [15,33].

Fig. 5 shows the cycle performance of Sn @ NPC and Sn @ CF electrodes. The improved cycle performance is exhibited in both higher capacity and better Coulombic efficiency. The charge capacity of Sn @ NPC in the first cycle is 1.68 mAh cm^{-2}, which is 20 times higher than that of Sn @ CF, and this ratio rises up to 90 at the 50th cycle, higher than the reported nano-architectured electrodes [15]. The reversible capacity retention of Sn @ NPC remains 58.5% after 10 cycles and 45.2% after 20 cycles. Except for the first several cycles, its Coulombic efficiency maintains above 95%. In comparison, the reversible capacity retentions of Sn @ CF after 10 cycles and after 20 cycles are 34.8% and 24.3%, respectively. Its Coulombic efficiency only fluctuates around 80%.

The good performance further demonstrates the merits of the special 3D nanostructured electrode developed from dealloying which contains both large channels and small pores. On one hand, the channels of hundreds of nanometers width could facilitate the solvent diffusion and mass transportation. The existence of large-scaled and uniformly distributed channels increases effective surface area of electrode by connecting more small pores on the channel walls with electrolyte. On the other hand, the small pores of tens of nanometers on the channel walls also contribute greatly by enlarging the surface area and accommodating more tin with less thickness. The large specific surface area enables higher active area during reaction and brings better capacity. The small thickness of tin relieves the mechanical stress associated with huge volume expansion during cycling. The nanopores could hold tin particles in case of delaminating from current collector even when cracks and pulverization occurred.

It needs to be point out that the conditions of electroless deposition of tin were not optimized in this work. The performance of Sn @ NPC could be further improved by developing the strategy of coating active material which will be one of our focuses in the future work.

4. Conclusions

The application of tin-coated nanoporous copper prepared by dealloying and electroless deposition in the lithium-ion battery demonstrates that three dimensional nanoporous electrode with large channels can be a promising strategy to prepare high performance anode material. The NPC with large surface area could work as both the current collector and substrate for the electrode. By comparing the voltage profiles and cycle performances with planar

Sn @ CF electrode, Sn @ NPC electrodes exhibit much higher capacity and better Coulombic efficiency. Special nanoporous structure with bimodal pore size distributions, i.e. large channels and small pores, give rise to the good performance.

Acknowledgments

This work was supported by the National Basic Research Program of China (973 Program) (2007CB936502), National Natural Science Foundation of China (50574008, 50954005) and National 863 Program (2006AA03Z230, 2008AA03Z208) of China.

References

[1] T. Brousse, O. Crosnier, X. Devaux, P. Paillard, J. Santos-Pena, D.M. Schleich, Powder Technol. 128 (2002) 124.
[2] M.-H. Park, M.G. Kim, J. Joo, K. Kim, J. Kim, S. Ahn, Y. Cui, J. Cho, Nano Lett. 9 (2009) 3844.
[3] M. Winter, J.O. Besenhard, Electrochim. Acta 45 (1999) 31.
[4] S. Yang, P.Y. Zavalij, M.S. Whittingham, Electrochem. Commun. 5 (2003) 587.
[5] S.D. Beattie, J.R. Dahn, J. Electrochem. Soc. 150 (7) (2003) A894.
[6] O. Mao, R.L. Turner, I.A. Courtney, B.D. Fredericksen, M.I. Buckett, L.J. Krause, J.R. Dahn, Electrochem. Solid-State Lett. 2 (1999) 3.
[7] A. Trifonova, M. Wachtler, M.R. Wagner, H. Schriettner, Ch. Mitterbauer, F. Hofer, K.C. Möller, M. Winter, J.O. Besenhard, Solid State Ionics 168 (2004) 51.
[8] K.D. Kepler, J.T. Vaughey, M.M. Thackeray, J. Power Sources 383 (1999) 81.
[9] T. Jiang, S. Zhang, X. Qiu, W. Zhu, L. Chen, J. Power Sources 166 (2007) 503.
[10] T. Jiang, S. Zhang, X. Qiu, W. Zhu, L. Chen, Electrochem. Commun. 9 (2007) 930.
[11] M. Valvo, U. Lafont, D. Munao, E.M. Kelder, J. Power Sources 189 (2009) 297.
[12] W. Choi, J.Y. Lee, B.H. Jung, H.S. Lim, J. Power Sources 136 (2004) 154.
[13] Y. Hu, Y. Guo, W. Sigle, S. Hore, P. Balaya, J. Maier, Nat. Mater. 5 (2006) 713.
[14] A.S. Aricò, P. Bruce, B. Scrosati, J.M. Tarascon, Nat. Mater. 4 (2005) 366.
[15] L. Bazin, S. Mitra, P.L. Taberna, M. Gressier, M.J. Menu, A. Barnabé, P. Simon, J.-M. Tarascon, J. Power Sources 188 (2009) 578.
[16] Z. Qi, C. Zhao, X. Wang, J. Lin, W. Shao, Z. Zhang, X. Bian, J. Phys. Chem. C 113 (2009) 6694.
[17] J. Zhang, P. Liu, H. Ma, Y. Ding, J. Phys. Chem. C 111 (2007) 10382.
[18] L. Chen, J. Yu, T. Fujita, M. Chen, Adv. Funct. Mater. 19 (2009) 1.
[19] L.Y. Chen, T. Fujita, Y. Ding, M.W. Chen, Adv. Funct. Mater. 20 (2010) 2279.
[20] J. Erlebacher, M.J. Aziz, A. Karma, N. Dimitrov, K. Sieradzki, Nature 410 (2001) 450.
[21] J.R. Hayes, A.M. Hodge, J. Biener, A.V. Hamza, K. Sieradzki, J. Mater. Res. 21 (2006) 2611.
[22] H. Li, A. Misra, J.K. Baldwin, S.T. Picraux, Appl. Phys. Lett. 95 (2009) 201902.
[23] Z. Zhang, Y. Wang, Z. Qi, J. Lin, X. Bian, J. Phys. Chem. C113 (2009) 1308.
[24] J.L. Murray, Int. Met. Rev. 30 (1985) 211.
[25] Y. Ding, Y.J. Kim, J. Erlebacher, Adv. Mater. 16 (2004) 1897.
[26] Y. Ding, J. Erlebacher, J. Am. Chem. Soc. 125 (2003) 7772.
[27] R.A. Huggins, J. Power Sources 13 (1999) 81.
[28] M. Inaba, T. Uno, A. Tasaka, J. Power Sources 146 (2005) 473.
[29] S.D. Beattie, T. Hatchard, A. Bonakdarpour, K.C. Hewitt, J.R. Dahn, J. Electrochem. Soc. 150 (2003) A701.
[30] W. Xu, N.L. Canfield, D. Wang, J. Xiao, Z. Nie, J. Zhang, J. Power Sources 195 (2010) 7403.
[31] X. Wang, X. Zhou, K. Yao, J. Zhang, Z. Liu, Carbon 49 (2011) 133.
[32] L.Y. Beaulieu, S.D. Beattie, T.D. Hatchard, J.R. Dahn, J. Electrochem. Soc. 150 (2003) A419.
[33] N. Pereira, L.C. Klein, G.G. Amatucci, Solid State Ionics 167 (2004) 29.